

The Initial-Final Mass Relation for Hydrogen-Deficient White Dwarfs*

JOSEPH W. BARNETT,¹ KURTIS A. WILLIAMS ¹, A. BÉDARD ² AND
MICHAEL BOLTE³

¹*Texas A&M University-Commerce
P.O. Box 3011
Commerce, TX 75429-3011, USA*

²*Département de Physique
Université de Montréal*

Montréal, QC H3C 3J7, Canada

³*University of California Santa Cruz
University of California
1156 High St.
Santa Cruz, CA 95064, USA*

(Accepted July 12, 2021)

Submitted to The Astronomical Journal

ABSTRACT

The initial-final mass relation (IFMR) represents the total mass lost by a star during the entirety of its evolution from the zero age main sequence to the white dwarf cooling track. The semi-empirical IFMR is largely based on observations of DA white dwarfs, the most common spectral type of white dwarf and the simplest atmosphere to model. We present a first derivation of the semi-empirical IFMR for hydrogen deficient white dwarfs (non-DA) in open star clusters. We identify a possible discrepancy between the DA and non-DA IFMRs, with non-DA white dwarfs $\approx 0.07 M_{\odot}$ less massive at a given initial mass. Such a discrepancy is unexpected based on theoretical models of non-DA formation and observations of field white dwarf mass distributions. If real, the discrepancy is likely due to enhanced mass loss during the final thermal pulse and renewed post-AGB evolution of the star. However, we are dubious that the mass discrepancy is physical and instead is due to the small sample size, to systematic issues in model atmospheres of non-DAs, and to the uncertain evolutionary history of Procyon B (spectral type DQZ). A significantly larger sample size is needed to test these assertions. In addition, we also present Monte Carlo models of the correlated errors for DA and non-DA white dwarfs in the initial-final mass plane. We find the

Corresponding author: Kurtis A. Williams

Kurtis.Williams@tamuc.edu, bedard@astro.umontreal.ca, bolte@ucolick.org

* Some of the data presented herein were obtained at the W.M. Keck Observatory, which is operated as a scientific partnership among the California Institute of Technology, the University of California and the National Aeronautics and Space Administration. The Observatory was made possible by the generous financial support of the W.M. Keck Foundation.

uncertainties in initial-final mass determinations for individual white dwarfs can be significantly asymmetric, but the recovered functional form of the IFMR is grossly unaffected by the correlated errors.

1. INTRODUCTION

White dwarfs (WDs) are the endpoint of stellar evolution for the vast majority of stars. These stellar remnants thus provide an observational anchor for studies of the late stages of stellar evolution and serve as forensic evidence of the complex physical processes active in the cores of asymptotic giant branch (AGB) stars.

Most ($\sim 80\%$) WDs are in the DA spectral class (e.g., [McCook & Sion 1999](#); [Kepler et al. 2019](#)), meaning that they are enshrouded by an opaque, nearly pure hydrogen layer with a mass of $\sim 10^{-10} - 10^{-4} M_{\text{WD}}$. These atmospheres are relatively straightforward to model at warmer temperatures, though recent progress in computational and laboratory physics has revealed systematic issues related to molecular interactions and line profiles that still are not fully understood (e.g., [Schaeuble et al. 2019](#); [Gomez et al. 2020](#)). Nonetheless, observations of DA WDs can be matched to model atmospheres to determine fundamental parameters such as the effective temperature, T_{eff} , and surface gravity, $\log g$, to relatively high precision (e.g., [Liebert et al. 2005](#); [Koester et al. 2009](#)).

The non-DA spectral classes are generally hydrogen deficient; most have atmospheres dominated by helium, though trace residuals of hydrogen or metals are often present (e.g., [Bergeron et al. 2019](#); [Genest-Beaulieu & Bergeron 2019a](#); [Coutu et al. 2019](#)). Most non-DA WDs also are suspected to change spectral type over their evolution due to atmospheric chemical stratification from the WD's high surface gravity and the establishment and growth of a surface convective zone; the exact evolution will depend on the mass of residual hydrogen (if any) and the thickness of the He layer (e.g., [Rolland et al. 2018](#); [Blouin et al. 2019](#); [Coutu et al. 2019](#); [Cunningham et al. 2020](#); [Bédard et al. 2020](#)).

A primary channel for non-DA WD production is via a late thermal pulse (LTP), a final burst of nuclear fusion that occurs during post-AGB evolution, or a very late thermal pulse (VLTP), a thermal pulse that occurs after the star has completed post-AGB evolution and entered the WD cooling track ([Schoenberner 1979](#); [Iben & Renzini 1982](#); [Iben et al. 1983](#)). These pulses consume or drive off nearly all remaining hydrogen and much of the remaining He shell (e.g., [Althaus et al. 2005](#); [Werner & Herwig 2006](#)).

Only a few LTPs and VLTPs have been directly observed: V4334 Sgr (Sakurai's Object; e.g., [Duerbeck & Benetti 1996](#); [Evans et al. 2020](#)) and V605 Aql (e.g., [Clayton & De Marco 1997](#); [Clayton et al. 2006](#)) are both suspected VLTPs (c.f. [Lau et al. 2011](#); [Clayton et al. 2013](#)), while FG Sge (e.g., [Gonzalez et al. 1998](#); [Lawlor & MacDonald 2003](#)) and V839 Aql (e.g., [Parthasarathy et al. 1993](#); [Reindl et al. 2014, 2017](#)) are

classified as likely LTPs. These thermal pulses do drive some additional mass loss; the ejected gas mass is measured at $\sim 10^{-5} - 10^{-4} M_{\odot}$ based on observations of ejecta in known (V)LTP events and in H-deficient planetary nebulae (e.g., Clayton et al. 2013; Guerrero et al. 2018; Evans et al. 2020; Schaefer et al. 2020). These thermal pulses send the star back toward the AGB in the Hertzsprung-Russell diagram, and total mass loss in the renewed post-AGB phase may approach to $\sim 10^{-2} M_{\odot}$ (Althaus et al. 2005). This additional mass loss would therefore only be a small fraction of the overall WD mass.

1.1. *The Initial-Final Mass Relation*

The initial-final mass relation (IFMR) quantifies the correspondence between the zero-age main sequence mass of a star and the mass of its WD progeny. The IFMR is generally assumed to be single-valued with negligible intrinsic scatter, weakly dependent on progenitor metallicity, and applicable only in the case of single star evolution or components of wide binary systems sufficiently separated that stellar interactions have no appreciable impact on each component’s evolution.

Theoretically, the IFMR can be calculated from evolutionary models of late stage AGB stars. This model IFMR takes the WD mass to be the core mass of a star at the cessation of primary nuclear burning stages; post-AGB mass loss and residual nuclear burning should have little effect on the remnant mass. In reality, physical limitations on models of processes such as core erosion during third-dredge up, convective and rotational mixing, and core growth during an uncertain number of successive thermal pulses limit the accuracy of these models (e.g., Cummings et al. 2019). For these reasons, many published modeled IFMRs tend to relate the progenitor star mass to the core mass at the first thermal pulse (e.g., Marigo et al. 2013).

The IFMR can also be derived semi-empirically through the observations of WDs in simple stellar systems such as open star clusters or wide binary systems in the field. In these cases the total system age is determined to reasonable accuracy through methods such as isochrone fitting (in an open cluster setting), and the cooling age of the white dwarf, τ_{cool} , can be determined by measuring the WD mass and effective temperature and then interpolating WD evolutionary model grids. The difference between the cluster age and τ_{cool} gives the nuclear lifetime of the progenitor star, τ_{nuc} , which corresponds to the progenitor star’s mass. This strong reliance on stellar and WD evolutionary models is why this observationally-based IFMR is known as “semi-empirical,” and a number of the most important systematics affecting the semi-empirical IFMR are quantified in Marigo et al. (2008) and still remain unresolved. Nonetheless, the semi-empirical IFMR has converged in recent years to a relatively tight relation with little intrinsic scatter (e.g., Cummings et al. 2018; Williams et al. 2018), at least for WDs arising from nearly solar metallicity progenitors that are analyzed using consistent methods with primarily self-consistent models.

Published semi-empirical IFMRs are almost entirely constructed from WDs of spectral type DA. For the $\approx 80\%$ of WDs that are DAs, this is not problematic. However, the non-DA WDs have undergone additional evolutionary processes that have resulted in the loss of most if not all of their outer H layer. It therefore is appropriate to consider the possibility that the IFMR for non-DA WDs may differ from the DA IFMR.

A priori one would expect little if any difference in the DA and non-DA IFMRs. The (V)LTP channel for production of non-DA WDs does not appear to result in significant mass loss from the evolving stellar core (e.g., Clayton et al. 2013; Guerrero et al. 2018; Evans et al. 2020; Schaefer et al. 2020). Empirically, the mean masses and overall mass distribution of field DA and non-DA WDs are observed to be very similar (spectroscopic mean masses of $0.615 M_{\odot}$ for DAs and $0.625 M_{\odot}$ for DBs; Genest-Beaulieu & Bergeron 2019b), though the DA distribution has a more substantial high-mass tail and a secondary peak at low mass due to binary star evolution (e.g., Bergeron et al. 1992; Falcon et al. 2010, 2012; Kleinman et al. 2013; Genest-Beaulieu & Bergeron 2019a).

No substantial attempt has been made at constructing the semi-empirical, non-DA IFMR to date. Non-DA WDs are rarer than DA WDs, so small number statistics will impact the results. More importantly, though, is the inherent difficulty in determining precise and accurate parameters for non-DA WDs (e.g., Tremblay et al. 2019; Bergeron et al. 2019; Genest-Beaulieu & Bergeron 2019a; Bédard et al. 2020). Processes such as van der Waals broadening, non-ideal atomic effects, and convective energy transport remain significant sources of uncertainty (e.g., Bergeron et al. 2011; Koester & Kepler 2015; Cukanovaite et al. 2018). Although substantial progress is being made through more complex computational efforts (Tremblay et al. 2020; Cukanovaite et al. 2021) and even laboratory studies of He at WD temperatures and pressures (Montgomery et al. 2020), observational determinations of non-DA WD parameters are simply subject to larger systematic uncertainty than those of DA WDs.

In this paper we present an attempt to construct the semi-empirical IFMR for non-DA WDs and compare that to both the DA semi-empirical IFMR and model IFMRs. We discuss the construction of a suitable non-DA sample from both previously-published and new observational data for open cluster non-DA WDs in Section 2. We then discuss new modeling of the observational uncertainties in the semi-empirical IFMR that could affect the interpretation of both the DA and non-DA IFMRs in Section 3. Finally, we discuss apparent differences between the DA and non-DA IFMRs that point out the need for additional study in Section 4.

2. OBSERVATIONS & ANALYSIS

2.1. *Sample Selection*

For this work, we scoured the literature for non-DA WDs in the fields of open star clusters. This search uncovered 13 non-DA WDs: two in the field of M34 (Rubin

Table 1. Astrometric Cluster Memberships of Non-DA WDs in Gaia EDR3

WD ID	Gaia EDR3	μ_α	$d\mu_\alpha$	μ_δ	$d\mu_\delta$	ϖ	$d\varpi$	Cluster Member?
	Source ID	mas yr ⁻¹	mas yr ⁻¹	mas yr ⁻¹	mas yr ⁻¹	mas	mas	
M34:LAWDS 7	337164523400019456	40.93	0.37	-18.37	0.35	5.85	0.36	No
M34:LAWDS 26	337191594578690560	9.0	1.5	-6.0	1.2	-0.9	1.1	No
Hyades:EGGR 316	3308403897837092992	95.286	0.039	-20.835	0.026	21.760	0.033	Yes
M47:DBH	3029912407273360512	-8.10	0.41	2.11	0.36	2.53	0.50	Yes
M67:WD21	604898490980773888	-11.4	0.43	-3.43	0.32	0.98	0.44	Yes
NGC6633:LAWDS 14	4477166581862730752	13.584	0.074	-78.115	0.071	10.709	0.067	No
NGC6633:LAWDS 16	4477253202776118016	-5.32	0.64	-9.62	0.60	-1.04	0.61	No

et al. 2008), one in the Hyades (e.g., Greenstein 1976; Eggen 1984; Tremblay et al. 2012), one in the field of M47 (Richer et al. 2019), two in the field of M35 (Williams et al. 2006, 2009), five in the field of M67 (Williams et al. 2018), and two in the field of NGC 6633 (Williams & Bolte 2007). We also include Procyon B, as its mass, effective temperature, and the total system age are tightly constrained (Bond et al. 2015, 2018; Sahlholdt et al. 2019), allowing us to consider the binary as a two-star cluster.

We then searched the Gaia EDR3 catalog (Gaia Collaboration et al. 2020) for each non-DA WD; seven WDs have tabulated proper motion and parallax measurements with the renormalized unit weight error (RUWE, Fabricius et al. 2020; Lindgren et al. 2020) ≤ 1.4 . We consider a WD to be a member of its respective open star cluster if the proper motion vectors and measured parallax are within 2σ of the cluster measurements tabulated in Gaia Collaboration et al. (2018a). These seven WDs, their Gaia EDR3 astrometry, and cluster membership determinations are presented in Table 1.

Due to their faint apparent magnitudes, four non-DA WDs in M67 do not have astrometry in the Gaia EDR3 catalog but are proper motion members of the cluster (Bellini et al. 2010; Williams et al. 2018): M67:WD18, M67:WD27, M67:WD30, and M67:WD31.

We exclude two non-DAs in the field of the open cluster Messier 35 due to a lack of proper motion measurements: M35:LAWDS 4, a DB WD, and M35:LAWDS 28, a hot DQ WD. Attempts to measure the proper motions of these two WDs are underway, and so we will wait to analyze these objects until the results are known.

Our final sample of cluster member non-DA WDs is given in Table 2.

2.2. White Dwarf Parameter Determination

2.2.1. Spectroscopic Observations & Reduction

Table 2. Non-DA WD Sample and Adopted Parameters

WD	Spectral Type	T_{eff} K	$\log g$ cgs	M_{WD} M_{\odot}	$\log \tau_{\text{cool}}$ log yr	Reference
EGGR 316	DBA	$15,129 \pm 361$	8.25 ± 0.07	0.74 ± 0.06	8.49 ± 0.07	1
M47:DBH	DBH	$32,100 \pm 2700$	8.73 ± 0.09	1.06 ± 0.05	7.84 ± 0.20	2
Procyon B	DQZ	7740 ± 50	8.02 ± 0.02	0.59 ± 0.01	9.12 ± 0.01	3,4
M67:WD18	DBA	$11,820 \pm 1313$	8.04 ± 0.24	0.61 ± 0.14	8.65 ± 0.21	This work
M67:WD21	DB	$30,765 \pm 2757$	7.84 ± 0.10	0.53 ± 0.05	6.93 ± 0.14	This work
M67:WD27	DC	7725 ± 520	7.65 ± 0.24	0.39 ± 0.11	8.91 ± 0.14	This work
M67:WD30	DB	$19,892 \pm 477$	8.19 ± 0.15	0.71 ± 0.09	8.04 ± 0.16	This work
M67:WD31	DC	8732 ± 777	7.22 ± 0.24	0.23 ± 0.11	8.58 ± 0.15	This work

References— (1) Rolland et al. (2018), (2) Richer et al. (2019), (3) Bond et al. (2015), (4) Bond et al. (2018)

We now discuss the spectral observations for the M67 non-DA WDs without previous parameter determinations. The 3500 – 5500 Å observations for the cluster sample WDs have already been detailed in Williams et al. (2009) and Williams et al. (2018). In summary, spectra were obtained over multiple observing runs using the blue channel of the Low Resolution Imaging Spectrometer (LRIS) on the Keck I telescope (McCarthy et al. 1998) and extracted using the onedspec and twospec packages in IRAF (Tody 1986, 1993). The extracted and co-added spectra have spectral resolutions of ≈ 8 Å FWHM.

WDs with helium-dominated atmospheres are often mixed with small amounts of hydrogen; the H/He ratio is important to quantify, as it can significantly affect the measured T_{eff} and $\log g$. Due to pressure effects, often only the H α Balmer line is clearly present in optical spectra.

In our previous publications on cluster WDs, the red channel spectroscopy covering the H α line were ignored, as H β and higher order Balmer lines are sufficient to constrain T_{eff} and $\log g$ in DA WDs. We therefore describe the red-channel LRIS spectral observations in more detail here; these data are used to constrain the atmospheric H/He ratio in our sample.

The red-channel data were obtained simultaneously with the blue-channel data for each WD. For all WDs, the D560 dichroic was used in combination with the 600 lines mm^{-1} , 7500 Å blaze grating. The central wavelength was set to 6245 Å, resulting in spectral coverage from the dichroic cutoff through ~ 7500 Å. Flat-fielding used the internal halogen lamps, and wavelength calibration was performed using arclamps of Ne, Hg and Zn. For all observations, either a 1''-wide longslit or a 1''-wide slitlet was used, resulting in a spectral resolution of 4.7 Å FWHM as measured from night sky emission lines.

The data were reduced and spectra extracted using IRAF. Multiple exposures were averaged using cosmic ray rejection and the spectra extracted using the IRAF twospec package. Relative flux calibration was performed using spectrophotometric stan-

Table 3. Dates and Instrumental Setup for Spectral Observations

WD	Obs. Date (UT)	Exp. Time (s)	Aperture	Spectrophotometric Standard Applied	Detector	S/N Ratio ^a
M67:WD18	2007 Jan 20	8 × 1200	1'' slitmask	Feige 34	Tektronix ^b	22
M67:WD21	2007 Jan 20	2 × 600	1'' longslit	Feige 34	Tektronix ^b	32
M67:WD27	2010 Feb 9	6 × 1140	1'' slitmask	G 191-B2B	LBNL ^c	22
M67:WD30	2010 Feb 9	6 × 1140	1'' slitmask	G 191-B2B	LBNL ^c	32
M67:WD31	2010 Feb 9	9 × 1140	1'' slitmask	G 191-B2B	LBNL ^c	21

^aper resolution element, measured at 6200 Å.

^bSee Oke et al. (1995) for details.

^cSee Rockosi et al. (2010) for details.

dards observed the same night with the same instrumental configuration. Details on variable observational parameters for each WD are given in Table 3. The spectra are plotted in Figure 1.

2.2.2. Spectroscopic and Photometric Model Fitting

In this section, we estimate the atmospheric parameters T_{eff} and $\log g$ of the M67 non-DA WDs by comparing photometric and spectroscopic data to the predictions of model atmospheres.

First, we analyze the photometric energy distribution of all five objects following the method described in Bergeron et al. (2019). Briefly, observed magnitudes are dereddened and converted into average fluxes, which are then fitted to a grid of theoretical fluxes using the least-square Levenberg-Marquardt algorithm. We rely on the model atmospheres of Genest-Beaulieu & Bergeron (2019a) and Blouin et al. (2019) for DB(A) and DC stars, respectively. We fit *ugr* photometry from Williams et al. (2018) for M67:WD18, M67:WD27, and M67:WD30, and *ugriz* photometry from the Sloan Digital Sky Survey Data Release 16 (Ahumada et al. 2020) for M67:WD21 and M67:WD31. We assume a distance of 883.0 ± 0.9 pc, obtained from the Gaia-derived cluster parallax $\varpi = 1.1325 \pm 0.0011$ mas (Gaia Collaboration et al. 2018b), and use the dereddening procedure of Harris et al. (2006). Four out of five objects do not show H α ; in these cases, we simply suppose a pure He composition. This assumption is entirely appropriate for DB WDs, as adding a trace of H at the detection limit has no effect on the measured parameters (see Genest-Beaulieu & Bergeron 2019b). However, this is not quite true for DC WDs: the derived mass can be very sensitive to the assumed H abundance (see Bergeron et al. 2019). Unfortunately, the uncertainty associated with the unknown H content of DC stars is unavoidable. For

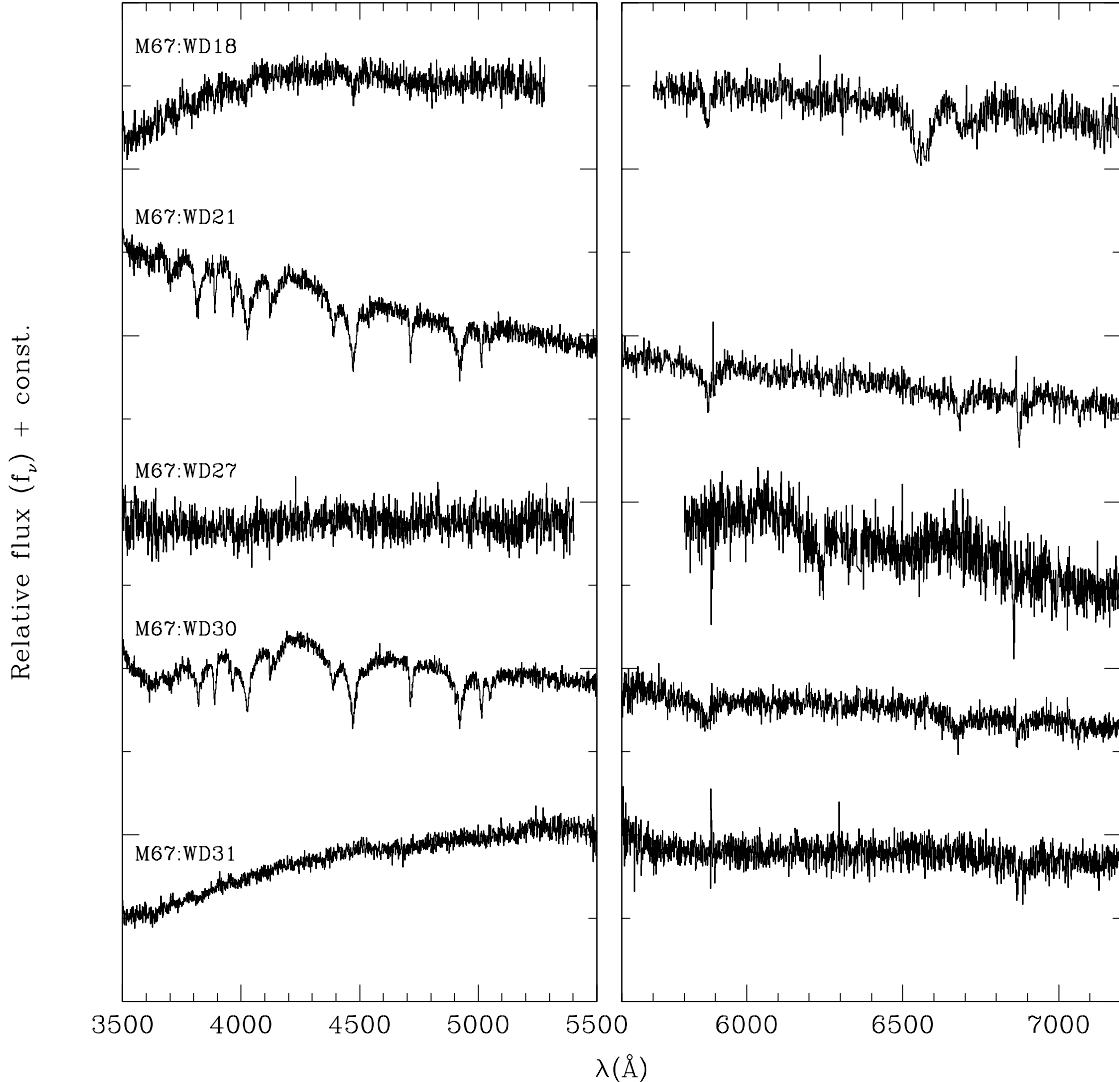


Figure 1. Spectra for the 5 non-DA WDs with new parameter determinations presented in this paper. Spectra are relatively flux calibrated and offset vertically by an arbitrary constant. *Left panel:* Blue-side spectra, previously published in [Williams et al. \(2018\)](#). *Right panel:* Red-side spectra, all newly presented here.

M67:WD18, which shows $H\alpha$, we experimented with various H abundances and we adopt $\log(H/He) = -5$ (see below). Our photometric fits are displayed in Figure 2.

Only two WDs (M67:WD21 and M67:WD30) exhibit He I lines strong enough to allow a meaningful spectroscopic analysis. For these objects, we also derive T_{eff} and $\log g$ values based on the spectroscopic fitting method of [Bergeron et al. \(2011\)](#). Briefly, the observed spectrum is first normalized to a continuum set to unity and then fitted to a grid of theoretical spectra using the least-square Levenberg-Marquardt algorithm. We employ the same model atmospheres mentioned above and again assume a pure He composition. We only include the blue spectrum, where most He I lines are located, in the fitting process. Unlike photometric fits which directly yield reliable uncertainties in T_{eff} and $\log g$, spectroscopic fits only provide formal fitting

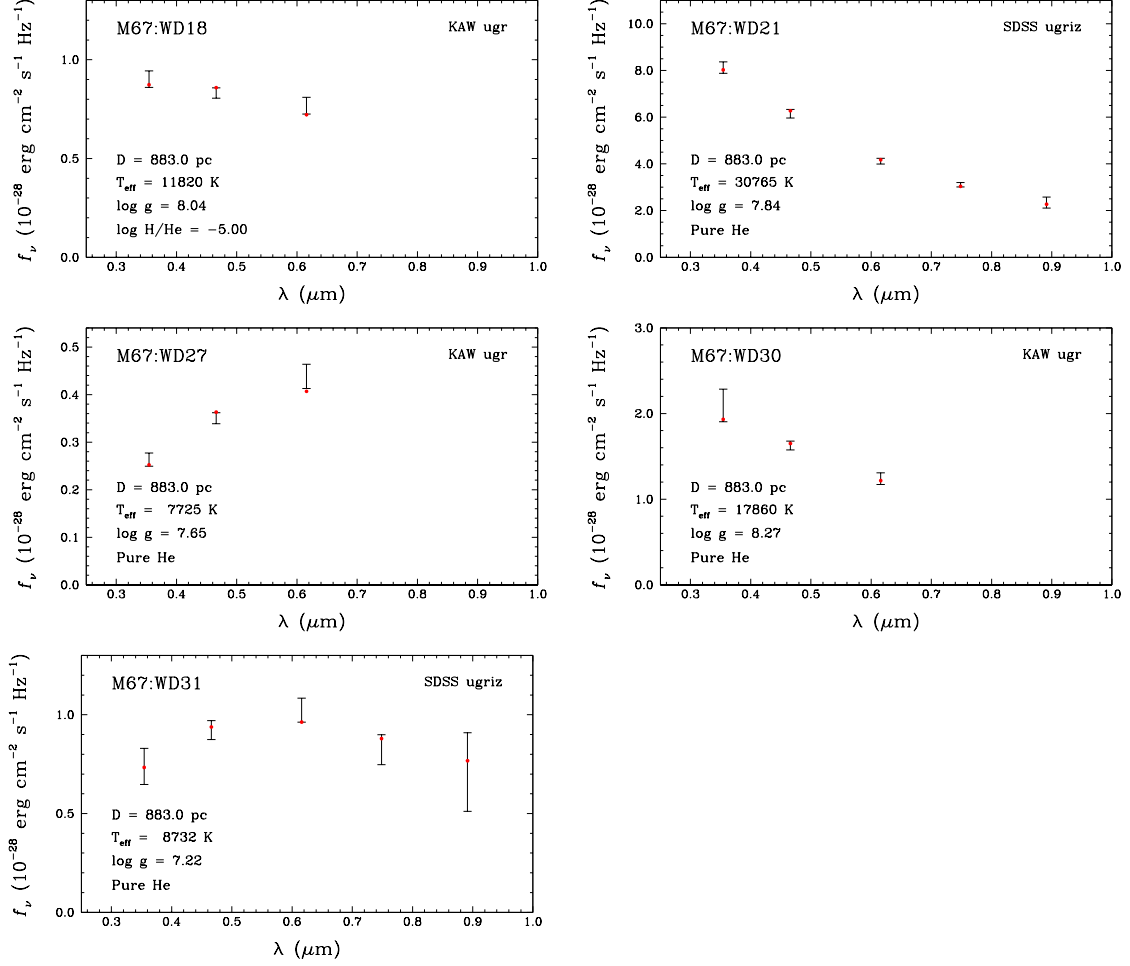


Figure 2. Fits of observed photometry (error bars) to fluxes derived from synthetic DB spectra (red points). The WD is identified in the upper left corner of each panel, and the best-fit solutions are given in the lower left. In the upper right, the source of the observed photometry is indicated; “KAW ugr” refers to *ugr* photometry from Williams et al. (2018), while “SDSS ugriz” refers to PSF *ugriz* photometry from the Sloan Digital Sky Survey Data Release 16 (Ahumada et al. 2020).

errors which measure the ability of the models to reproduce the data and are often smaller than the true uncertainties in estimating the physical parameters. A more realistic estimate of the uncertainties can be obtained by analyzing multiple spectra of the same star and computing the standard deviation of the resulting parameters. Since we have only one spectrum for each object, we conservatively adopt the average spectroscopic uncertainties of the DB sample of Genest-Beaulieu & Bergeron (2019a): $\sigma_{T_{\text{eff}}} = 0.024 \times T_{\text{eff}}$ and $\sigma_{\log g} = 0.15$ dex. Our spectroscopic fits for M67:WD21 and M67:WD30 are shown in Figures 3 and 4, respectively.

From each set of T_{eff} and $\log g$, we compute the corresponding stellar mass and cooling age using WD evolutionary sequences. For the DB(A) stars M67:WD18, M67:WD21, and M67:WD30, we rely on the C/O core, thin H envelope models of Bédard et al. (2020). For the DC stars M67:WD27 and M67:WD31, which have

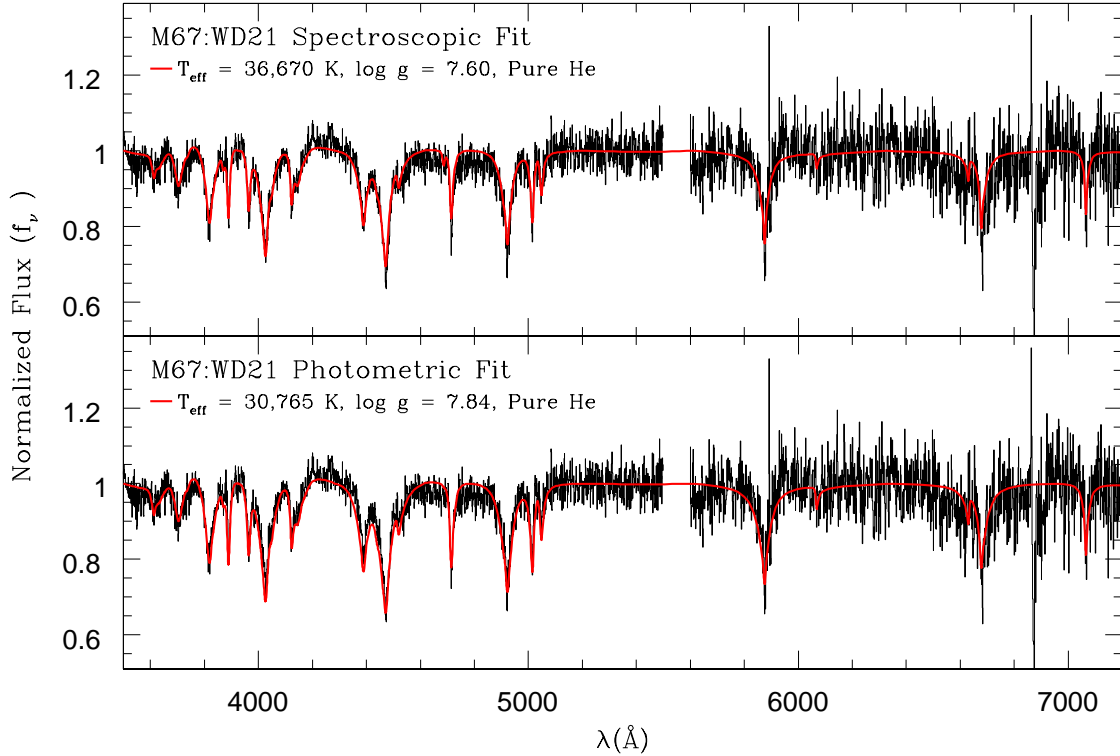


Figure 3. Comparison of spectral observations of M67:WD21 with model spectra. (*Top*): The normalized, observed spectrum (black) is compared to the best-fitting spectroscopic model (red). Most of the He I line core strengths are underpredicted. (*Bottom*): The normalized observed spectrum with the synthetic spectrum for the best-fit photometric model overlaid. Qualitatively the line cores appear to be better matched, but the strength of gravity-sensitive lines is overpredicted.

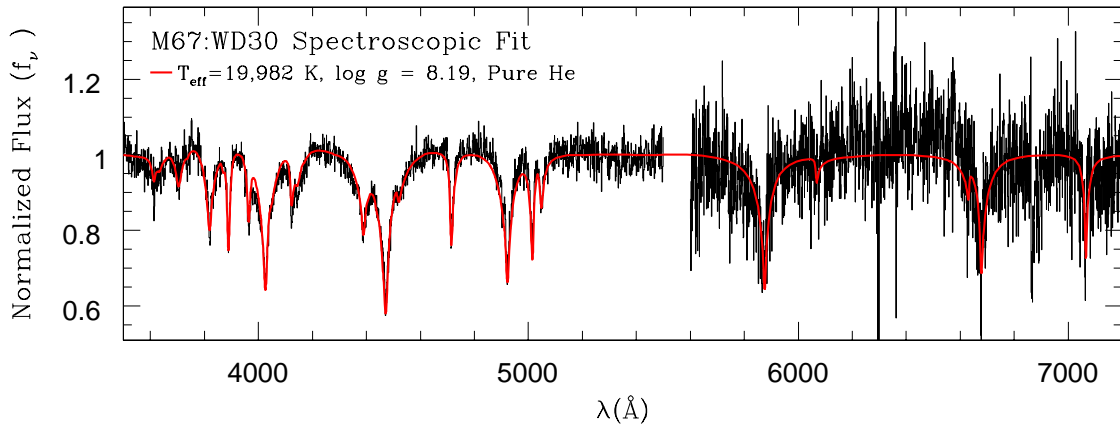


Figure 4. The normalized observed spectrum of M67:WD30 (black) compared to the best-fit normalized spectroscopic model (red). Only the blue spectrum was used in fitting. The dip in the red spectrum starting at 6861 Å is the telluric B band. Qualitatively the fit appears excellent, even on the red side.

unusually low $\log g$ values, we use instead the He core models of [Althaus et al. \(2013\)](#). The results of our analysis are presented in Table 2. For the two objects with both spectroscopic and photometric parameters, we give the adopted solution (see below).

2.2.3. Notes on Individual Objects

M67:WD21—This hot, bright WD, also known as LB 3600, was first identified as a DB by [Fleming et al. \(1997\)](#). Spectroscopic fitting provided two potential solutions, one on each side of the maximum strength of the He I lines, but the hot solution is clearly preferred by the photometry. Comparison of the observed spectrum to the best-fitting model shows a poor fit to the cores of most absorption lines (Figure 3, top panel). This WD has SDSS photometry, and comparison of the observed spectrum to a synthetic spectrum with the photometric parameters shows a closer though still imperfect match to the line cores (Figure 3, bottom panel). However, the photometric model does a poorer job of matching the gravity-sensitive 4388 Å He I line.

For this work, we adopt the photometric solution, in part because of the better match to the line cores, and in part because the larger error bars of the photometric fit more accurately define the uncertainty around the parameters for this WD. A higher signal-to-noise spectrum would be useful for this DB.

M67:WD30—This DB gives the most satisfying spectral fit of the entire sample, as shown in Figure 4. Although the spectral fit was determined only by the blue side spectrum, the synthetic spectrum for the red side qualitatively agrees with the observations very well. The photometric parameters (Figure 2) are entirely consistent with the spectroscopic parameters within the uncertainties. In the following, we adopt the spectroscopic solution. The derived WD mass of $0.71 \pm 0.09 M_{\odot}$ is larger than the masses of most M67 WDs; this WD could therefore be the remnant of blue straggler evolution (see discussion in [Williams et al. 2018](#)).

M67:WD18—We classify this WD as a DBA due to the presence of a very strong H α absorption line. Because this WD exhibits relatively weak He I lines, we did not fit the spectrum and instead used the photometric data from [Williams et al. \(2018\)](#) to derive the parameters given in Table 2. We also retrieved photometry for this star from the Pan-STARRS1 3π stack images photometric catalog ([Chambers et al. 2016](#)); these data prefer a slightly cooler temperature ($T_{\text{eff}} \approx 10,000$ K) but lack the significant constraints provided by the u -band.

In Figure 5, we compare the observed spectrum to the synthetic spectra computed from the photometric solutions for assumed H abundances of $\log(\text{H}/\text{He}) = -5$ and $\log(\text{H}/\text{He}) = -4$. Neither of these reproduce the observed spectrum well, and different assumed abundances are even poorer matches to the observed spectrum.

Assuming that M67:WD18 is a single He-rich WD, the breadth of the H α line requires van der Waals broadening to explain; this broadening occurs in mixed atmospheres but at much lower T_{eff} than indicated by the photometry. A cooler, higher-pressure atmosphere would also explain the weakness or absence of the H β absorption

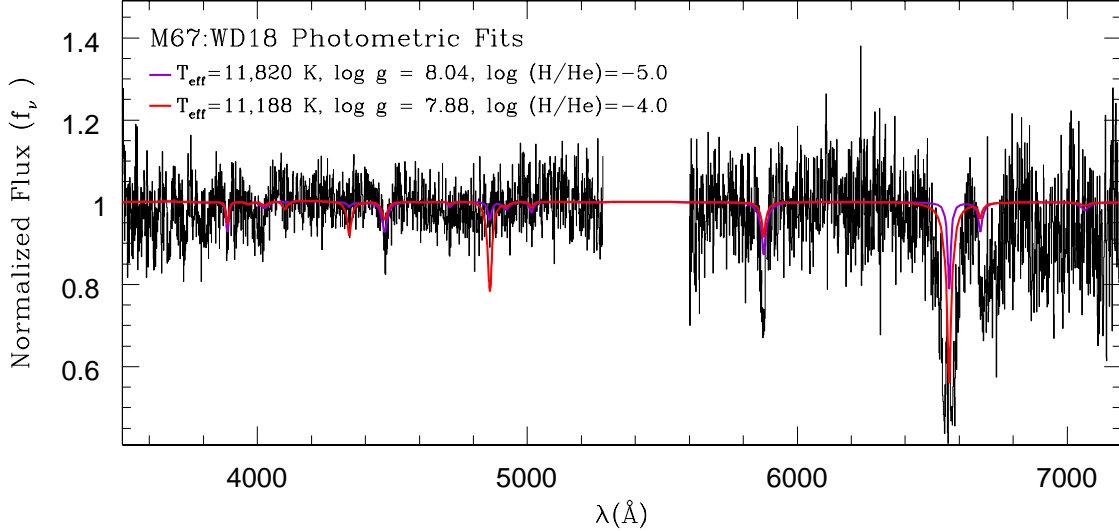


Figure 5. The normalized, observed spectrum of M67:WD18 (black) overlaid with normalized synthetic spectra for purely photometric WD parameter fits with assumed hydrogen abundances of $\log(\text{H}/\text{He}) = -5.0$ (violet line with shallower $\text{H}\alpha$) and $\log(\text{H}/\text{He}) = -4.0$ (red curve with deeper $\text{H}\alpha$). Neither synthetic spectrum matches the observed spectral features well, and changes to T_{eff} , $\log g$, and $\log(\text{H}/\text{He})$ cannot simultaneously match all significant spectral features. We therefore suspect that this is a composite spectrum.

line. However, this is completely at odds with the presence of He I lines in the spectrum.

We therefore suspect that the spectrum of M67:WD18 is composite. Some spectral features, such as the absorption from $\sim 6650 - 6800 \text{ \AA}$, look to be molecular bands from a cool K or M dwarf companion, while the width and depth of $\text{H}\alpha$ seem more indicative of a cool DA companion. The WD is unresolved and has no nearby neighbors in our deep MMT imaging (Williams et al. 2018). The parameter space is too unconstrained by the available data to (a) confirm that it is indeed a multiple star system, and (b) provide T_{eff} and $\log g$ for the individual components. As the $\text{H}\alpha$ feature likely does not originate from the He-rich WD, we simply adopt the photometric solution for a typical H abundance of $\log(\text{H}/\text{He}) = -5$. We are reluctant to include this WD in an IFMR that assumes single star evolution, but its inclusion or exclusion does not affect our conclusions.

2.2.4. Non-DA Parameters from the Literature

Three of the WDs in our sample have well-determined parameters already published. We now discuss each of these briefly in order to justify our adopted parameters for each WD.

Procyon B—Procyon B is a DQZ WD; its contribution to the IFMR was first discussed in detail by Liebert et al. (2013), who used a spectroscopic mass determination of $M = 0.553 \pm 0.022 M_{\odot}$ and a total system age of $1.87 \pm 0.13 \text{ Gyr}$. This resulted in a derived progenitor mass for Procyon B of $2.59^{+0.44}_{-0.26} M_{\odot}$.

Precision astrometry of the Procyon system by [Bond et al. \(2015\)](#) and [Bond et al. \(2018\)](#) gives a significantly higher mass for Procyon B of $0.592 M_{\odot}$. In addition, asteroseismic analyses of Procyon A prefer older system ages. [Guenther et al. \(2014\)](#) derive an age of 2.4–2.8 Gyr using YREC stellar evolutionary models ([Demarque et al. 2008](#)), while [Sahlholdt et al. \(2019\)](#) derive a benchmark age range of 1.5 – 2.5 Gyr from a variety of stellar models, though the majority of models they consider prefer ages of 2.0 – 2.5 Gyr.

For this work, we adopt the dynamical mass for Procyon B of $M = 0.592 \pm 0.013 M_{\odot}$ ([Bond et al. 2018](#)) and a spectroscopically-derived $T_{\text{eff}} = 7740 \pm 50$ K ([Provencal et al. 2002](#)). [Coutu et al. \(2019\)](#) use a spectrophotometric fitting method to find a cooler $T_{\text{eff}} = 7585 \pm 33$ K, though this results in a significantly lower mass ($0.554 \pm 0.013 M_{\odot}$) than the dynamical mass. If we combine this more recent T_{eff} determination with the dynamical mass, the model photometry would not agree with the known luminosity of Procyon B. For that reason, we choose to adopt the [Provencal et al. \(2002\)](#) T_{eff} . We note that if the T_{eff} from [Coutu et al. \(2019\)](#) is more precise, then the discrepancy of Procyon B with the DA IFMR would be even more severe; see Section 4.1.

For the sake of consistency in our IFMR calculations, we adopt an asteroseismic age of 2.25 ± 0.25 Gyr – [Sahlholdt et al. \(2019\)](#) derive an age of 2.2 – 2.3 Gyr using PARSEC models, but we inflate the uncertainty to reflect the range in the majority of their models (2.0 – 2.5 Gyr). Finally, we adopt a metallicity of $[\text{Fe}/\text{H}] = -0.05 \pm 0.03$ ([Kervella et al. 2004](#)).

EGGR 316—*EGGR 316* is a well-studied DBA in the Hyades open star cluster. The recent spectral analysis by [Rolland et al. \(2018\)](#) obtains $T_{\text{eff}} = 15,120 \pm 361$ K, $\log g = 8.25 \pm 0.09$, and $\log(\text{H}/\text{He}) = -4.68 \pm 0.06$; these were derived using the same methodology as our spectral parameters in Section 2.2. For the Hyades, we adopt the PARSEC-derived cluster age of 700 ± 25 Myr ([Cummings et al. 2018](#)).

DBH in Messier 47—[Richer et al. \(2019\)](#) identify a massive magnetic helium-atmosphere WD (spectral type DBH) in the open star cluster Messier 47, Gaia 3029912407273360512, which for simplicity we nickname M47:DBH. We adopt their spectroscopic parameters, which were determined via the same methodology as our DB spectral parameters in Section 2.2: $T_{\text{eff}} = 32,100 \pm 2700$ K and $M = 1.06 \pm 0.05 M_{\odot}$. For the cluster age and metallicity, we adopt the PARSEC-based determinations of [Gaia Collaboration et al. \(2018a\)](#): $\log \text{age (yr)} = 8.11^{+0.08}_{-0.06}$ and $[\text{Fe}/\text{H}] = +0.09$.

The adopted cluster parameters are summarized in Table 4.

3. MODELING UNCERTAINTIES IN THE IFMR

Traditionally, the uncertainties in the location of WDs in the IFMR are portrayed by orthogonal error bars in M_i and M_f (e.g., [Williams et al. 2009](#); [Cummings et al. 2018](#)). However, in many cases the uncertainties in these quantities are highly correlated.

Table 4. Adopted Cluster Parameters

Cluster	age (Myr)	[Fe/H]	Reference
Hyades	700 ± 25	+0.15	1
M47	129^{+26}_{-17}	+0.09	2
Procyon	2250 ± 250	-0.05	3,4
M67	3540 ± 150	+0.02	5

References— (1) Cummings et al. (2018) (2) Gaia Collaboration et al. (2018a) (3) Sahlholdt et al. (2019) (4) Kervella et al. (2004) (5) Bonatto et al. (2015)

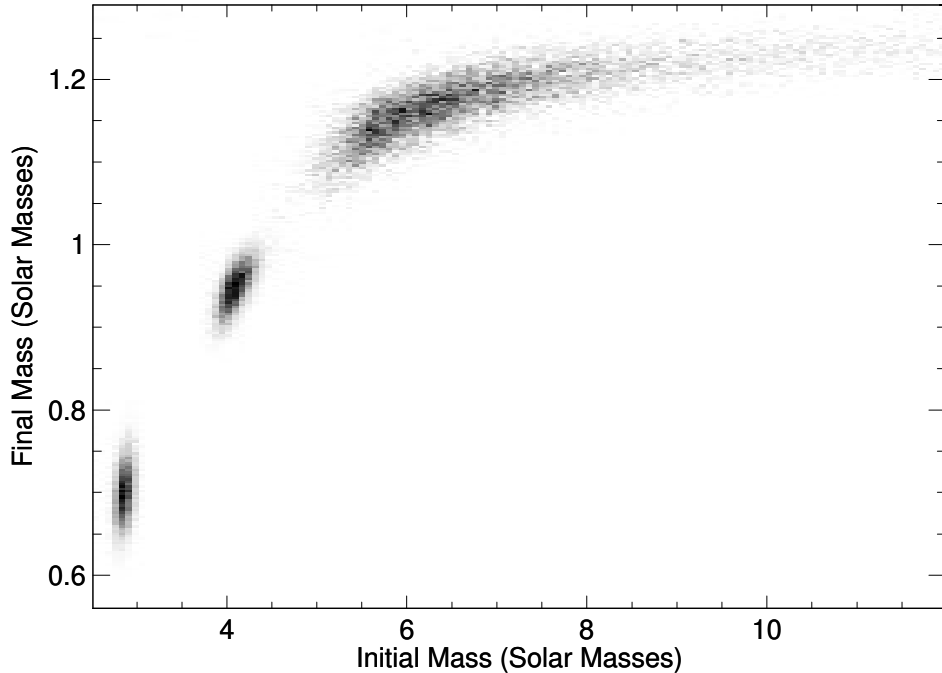


Figure 6. Examples of the correlated errors in the IFMR for three DA WDs with high signal-to-noise observations: WD 0421 + 162 (bottom left), NGC 3532 RK 1 (center), and NGC 2168:LAWDS 2 (top right). Grayscale indicates the density of points resulting from 10^4 simulated observations of each WD using published errors in T_{eff} and $\log g$, and assuming no uncertainty in the cluster age. This figure originally appeared in Williams (2020); reproduced with permission.

A higher-mass WD typically requires a larger τ_{cool} to reach a given T_{eff} , which for a given cluster age implies a shorter nuclear lifetime for the progenitor, which in turn implies a higher progenitor mass. The slope of this correlation in the IFMR plane varies from WD to WD and is highly sensitive to the ratio of the uncertainty in τ_{cool} to the derived progenitor nuclear lifetime (Figure 6, Williams 2020).

Table 5. PARSEC-derived WD Progenitor Masses

WD	M_f	M_i	$dM_{i,\text{rand}}$	$dM_{i,\text{sys}}$
	M_\odot	M_\odot	M_\odot	M_\odot
Hyades:EGGR 316	0.74 ± 0.06	3.26	+0.16 -0.12	+0.07 -0.07
M47:DBH	1.06 ± 0.05	6.73	+2.80 -1.10	+1.12 -1.02
Procyon B	0.59 ± 0.01	2.37	+0.03 -0.03	+0.26 -0.18
M67:WD18	0.61 ± 0.14	1.58	+0.05 -0.03	+0.03 -0.03
M67:WD21	0.53 ± 0.05	1.51	+0.01 -0.01	+0.02 -0.02
M67:WD30	0.71 ± 0.09	1.52	+0.01 -0.01	+0.02 -0.02

NOTE— M_f is repeated from Table 2 for the reader’s convenience. Uncertainties are 68th percentile. Random errors include only propagated uncertainties in WD parameters; systematic errors include only cluster age uncertainty.

3.1. Model Errors for Individual White Dwarfs

We therefore set out to determine the actual shape of the M_i , M_f uncertainties for each of the non-DA WDs included in our semi-empirical IFMR via a Monte Carlo simulation. The calculation consists of 10^6 simulated measurements of each WD’s T_{eff} and $\log g$. The values of each are drawn randomly assuming a Gaussian distribution centered on the best fit T_{eff} and $\log g$ with a standard deviation equal to the stated uncertainties on each parameter. We assume the T_{eff} and $\log g$ are uncorrelated measurements, though in fact they are weakly correlated in many cases. Each simulated T_{eff} and $\log g$ is then run through the same series of model-dependent calculations to derive M_i and M_f .

For each simulated observation, the cluster age is randomly chosen from a flat distribution centered on the adopted cluster age. The best choice of age uncertainty distribution is not obvious *a priori*, and many sources of open cluster ages do not specify the uncertainty distribution. We tested four different error assumptions – flat and Gaussian distributions in both linear and logarithmic distributions – and the assumed distribution has no impact on our qualitative conclusions for this work.

In Figure 7, we present a density plot of the simulated M_i , M_f pairs for each WD. Error bars indicate the extent of 68% of the simulated points centered on the median initial and final mass values for each WD; these median values are presented as the best-fit solutions in Table 5. This analysis was accomplished by slightly modifying the IDL procedure `density.pro` (Arendt 2006).

Generally, the location of the M_i , M_f point calculated from the best-fit WD parameters and assumed cluster age tend to lie at higher M_i values than the highest density of simulated output points. This raises a concern that the derived M_i , M_f point may not accurately reflect the location of the true IFMR.

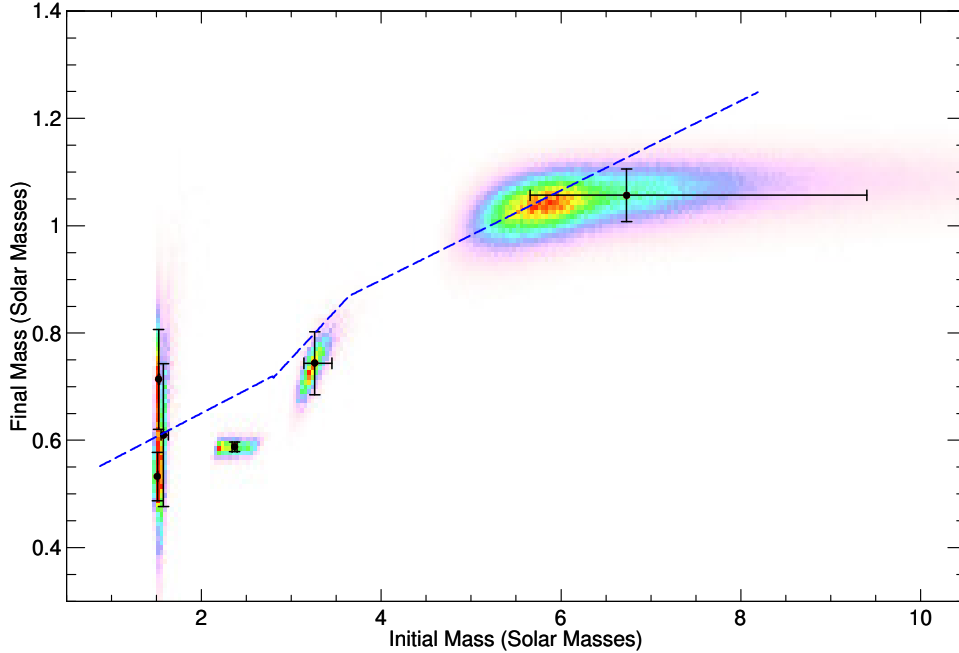


Figure 7. Comparison of the semi-empirical initial-final mass relation for non-DA white dwarfs (black points) to the piece-wise linear DA IFMR (Cummings et al. 2018, dashed blue line). Black points indicate the data from Table 5, while the colored shading indicates the density of points in our simulation of IFMR uncertainties. The density shading is rescaled for each WD such that the most common outcomes are shaded red. The error bars indicate the range encompassed by 68% of each WD’s simulations. In spite of large uncertainties, the non-DA WDs appear to lie below the DA IFMR.

Additional testing revealed that the apparent discrepancy between the calculated M_i, M_f location and the simulation density distribution is almost exclusively due to the steep slope of the relation between progenitor masses and nuclear lifetimes; the location of the calculated M_i, M_f point accurately reflects the median of both parameters in the simulations.

3.2. Modeling Uncertainty in the Shape and Location of the IFMR

To be certain that the correlated errors and the offset between the median and mode of the simulated uncertainties does not bias the derivation of the semi-empirical IFMR, we conducted a further simulation of WD observations in order to compare an input IFMR with a recovered “observed” IFMR.

Our simulation is designed to determine if the correlated errors result in a bias in the derived shape and slope of the IFMR. We begin by generating stellar populations in 7 simulated cluster with known log ages = 7.75 and 8.00 – 9.67 in 0.33 dex increments. Within each cluster, we draw 10^5 stars with initial masses $\leq 8 M_\odot$ following a Salpeter IMF distribution and nuclear lifetimes shorter than the cluster age; nuclear lifetimes are determined from PARSEC v. 1.2S models with $Z = 0.019$ (Bressan et al. 2012;

Chen et al. 2014; Chen et al. 2015), retrieved using the CMD 3.4 interface¹. Each input star is assumed to become a single WD with a mass given by the piecewise linear PARSEC IFMR of Cummings et al. (2018). This input IFMR is derived using primarily DA WDs, so the thick H envelope, C/O core evolutionary models of Bédard et al. (2020) are used to determine the T_{eff} and $\log g$ for each WD given the known cooling time (cluster age minus nuclear lifetime). For now we ignore the complication that WDs resulting from single-star evolution with masses $\gtrsim 1.05 M_{\odot}$ likely have oxygen-neon cores, not C/O cores.

Our next step is to model the uncertainties in T_{eff} and $\log g$ resulting from spectral observations of each generated WD. While in reality these uncertainties will vary depending on the details of observations, we chose to use typical uncertainties published in the recent literature for open cluster WDs: $\sigma_{\log g} = 0.05$ dex and $\sigma_{T_{\text{eff}}} = 0.025 \times T_{\text{eff}}$. The observed parameters, $T_{\text{eff,obs}}$ and $\log g_{\text{obs}}$ are then calculated by drawing the error in each value from a Gaussian distribution with a standard deviation of the adopted uncertainty in each parameter.

Each simulated WD is then run through our IFMR machinery to determine its observed M_i and M_f . Because spectroscopically derived parameters for cool DAs are affected by systematic issues in model atmospheres, and because these cool WDs are generally fainter than observational magnitude limits, we discard (without redrawing) any simulated WDs with $T_{\text{eff,obs}} < 12,000$ K. We also discard without redrawing all simulated WDs with derived cooling ages longer than the input cluster age, since the calculated nuclear lifetime of the progenitor would be negative.

The recovered IFMR are shown in Figure 8 as a logarithmic density plot compared to the input IFMR, indicated by the dashed line. We see that the recovered IFMR is in excellent qualitative agreement with the input IFMR, though with a slight asymmetric tail to higher recovered initial masses at the high M_i end. The lowest-density regions (blue and purple shades) of the recovered IFMR indicate a small number of simulations per pixel and are associated with simulated WDs with $\tau_{\text{cool}} > \tau_{\text{nuc}}$.

Based on these simulations, we conclude that the correlated uncertainties in initial and final masses for individual WDs introduce no significant biases in shape and location of the semi-empirical IFMR recovered from an ensemble of WDs, at least when only uncertainties in the observations of T_{eff} and $\log g$ are considered. Uncertainties in the ages of the input clusters will introduce systematic errors for all WDs in a given cluster, and that effect has not been considered here.

4. THE NON-DA INITIAL-FINAL MASS RELATION: DISCUSSION

With a modicum of confidence in our understanding of the uncertainties, we can now compare the position of non-DA WDs in the initial-final mass plane to the semi-empirical IFMR derived from (primarily) DA WDs. We exclude M67:WD27 and M67:WD31 from the IFMR analysis, as the WD masses derived from their low $\log g$

¹ stev.oapd.inaf.it/cgi-bin/cmd

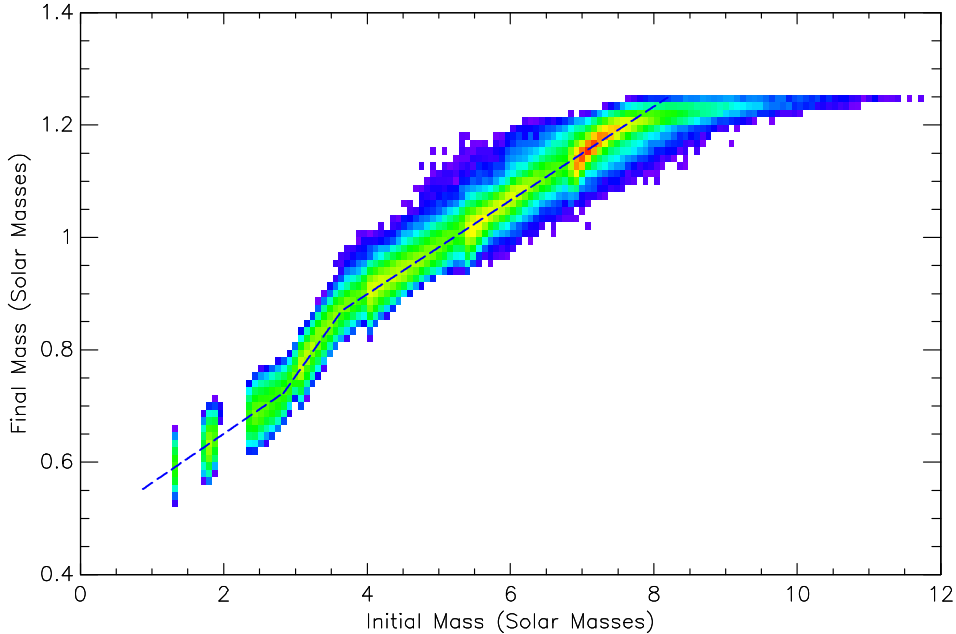


Figure 8. A density plot of the recovered semi-empirical IFMR compared with the input IFMR (dashed line, from Cummings et al. 2018) from the Monte Carlo simulation described in the text. The density gradient is logarithmic. Based on these results, we conclude that the correlated errors in the IFMR for individual WDs resulting from the uncertainties in T_{eff} and $\log g$ measurements such as those in Figure 6 do not translate to significant biases in the shape and location of the ensemble semi-empirical IFMR, at least when uncertainties in assumed cluster ages are ignored.

values are sufficiently low to indicate that either these two DCs are the He-core results of binary evolution, or that they are not bona fide cluster members.

In Figure 7, we compare the non-DA WDs from this analysis to the piecewise-continuous linear fit derived from Cummings et al. (2018). For both sets of data, we use the PARSEC stellar evolutionary models for deriving both star cluster ages and the progenitor masses as a function of nuclear lifetimes. We find that the DBs are consistent with the DA-derived IFMR, but that Procyon B, a DQZ, has a mass $0.1 M_{\odot}$ lower than the DA IFMR.

4.1. The outlier Procyon B

This apparently low mass for Procyon B has been noted before (e.g., Liebert et al. 2013), and potential explanations are discussed thoroughly in Bond et al. (2015). In summary, the parameters of Procyon A and Procyon B as determined from precision astrometric measurements and astroseismic observations of Procyon A are consistent and well constrained. It therefore is not possible to reconcile the location of Procyon B in the initial-final mass plane with the DA IFMR from measurement errors alone.

Bond et al. (2015) suggest two solutions to the Procyon problem. First, perhaps the Procyon system underwent significant binary interactions in the past. In summary, the separation of the binary components prior to mass loss from Procyon B’s pro-

genitor star would have been ~ 5 AU. This is large enough that the pair would not have shared a common envelope, but tidal interactions and mass transfer from the post-main sequence wind of Procyon B may have occurred. If the total mass transfer were significant, the evolution of Procyon A would be sped up, making the system appear substantially younger than it actually is.

The second suggestion of Bond et al. (2015) is that the apparently low mass of Procyon B is simply due to large intrinsic scatter in the IFMR, i.e., there is some spread in the WD mass resulting from a progenitor star of a given mass. This suggestion is based on the apparent scatter in the semi-empirical IFMR of Ferrario et al. (2005).

We are skeptical of this latter hypothesis. Cummings et al. (2015) illustrate that this apparent scatter is significantly reduced when WD parameters and cluster ages are determined in an internally consistent manner, which was not the case in Ferrario et al. (2005). Further, Williams et al. (2018) show that the measured standard deviation of WD masses in M67 is $\approx 0.04 M_{\odot}$ once low-mass He core WDs and abnormally massive WDs potentially resulting from blue stragglers are excluded from the sample; this scatter is consistent with the observational uncertainties and constrains any intrinsic scatter in the M67 IFMR to be less than $0.02 M_{\odot}$.

Procyon B is significantly cooler than the other non-DA WDs analyzed here. It also has a spectral type of DQZ in contrast to the DAs and other non-DAs in the IFMR; the models used to derive Procyon B's temperature and cooling age could be systematically off. Indeed, Coutu et al. (2019) argue that there appears to be a systematic shift in the parameters derived for DQ WDs, potentially due to problems with UV carbon opacities in the model atmosphere. Other systematic effects such as gravitational settling of ^{22}Ne , not included in the evolutionary models of Bédard et al. (2020), could also be affecting the derived cooling age (e.g., García-Berro et al. 2008).

Yet even if Procyon B's cooling age is treated as unknown, its initial mass is constrained by the age of Procyon A (assuming no significant binary interactions) to be $\gtrsim 1.5 M_{\odot}$, and its WD mass would still be below the DA IFMR, though at a lower significance. For these reasons, neither intrinsic scatter nor observational scatter in the IFMR seem likely explanations for Procyon B.

4.2. Differences in the DA and non-DA IFMR?

A third possible explanation for the position of Procyon B compared to the semi-empirical IFMR is that the non-DA IFMR differs from the DA IFMR. Figure 9 compares the semi-empirical non-DA IFMR and uncertainties with the DA IFMR of Cummings et al. (2018), the model-derived non-DA IFMR of Althaus et al. (2009), the functional fit to model-based core masses of stars at the first thermal pulse from Marigo et al. (2013), and the DA IFMR arbitrarily shifted by $0.07 M_{\odot}$ to lower WD masses. With the exception of M67:WD30, all of the non-DA WDs appear most

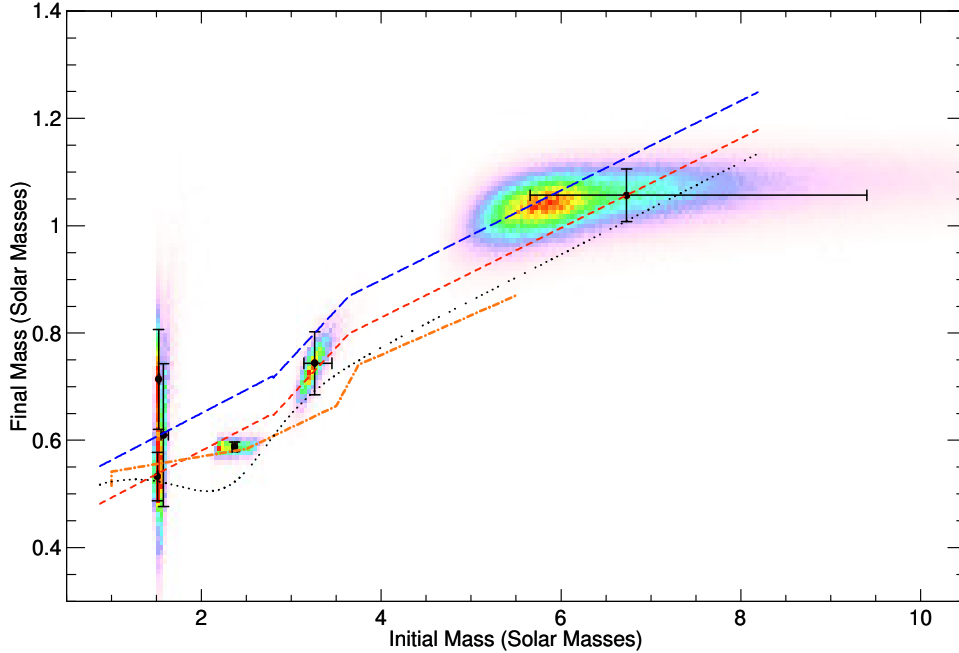


Figure 9. The same non-DA IFMR as in Figure 7 compared to various IFMRs: the Cummings et al. (2018) semi-empirical IFMR for DAs (blue, long-dashed line), the Cummings et al. (2018) IFMR shifted to lower final masses by $0.07 M_{\odot}$ (red, short-dashed line), the modelled non-DA IFMR of Althaus et al. (2009) (orange dash-dotted line), and the core mass at first thermal pulse relation from Marigo et al. (2013) (black dotted curve). With the exception of M67:WD30, all the non-DA WDs in this sample including Procyon B are most consistent with the shifted DA IFMR, and reasonably consistent with the model-based IFMRs.

consistent with the shifted IFMR and are consistent within errors of the two model-based curves.

If the $0.07 M_{\odot}$ offset we observe is indeed physical in nature, an obvious potential explanation would be enhanced mass loss during the (V)LTP and the rejuvenated star’s additional stint on the post-AGB evolutionary track. Since the maximum mass of a WD’s helium layer is $\approx 10^{-2} M_{\text{WD}}$, much of the required additional $0.07 M_{\odot}$ of mass loss would have to come from the carbon-oxygen core of the star. This mass loss could be observable due to enhanced dust formation. However, the observed mass lost following these late thermal pulses ($\sim 10^{-4}$) is more than two orders of magnitude lower than the observed difference we suggest might exist. Althaus et al. (2005) report their models show an additional $0.013 M_{\odot}$ of mass loss during the hot post-AGB evolution following a VLTP, but even this mass loss would be nearly an order of magnitude too small. For this reason and additional considerations outlined below, we have serious doubts about the physical reality of a significant difference between the DA and non-DA IFMRs.

Even if the mass loss during the (V)LTP and renewed post-AGB evolution of the star is enhanced, or even if some other physical mechanism during stellar evolution

affects the mass of non-DAs, the difference in WD masses hinted at by the non-DA IFMR would be in conflict with multiple measurements of the mean masses of DA and non-DA WDs, which typically are observed to be the same within 0.01 or 0.02 M_{\odot} .

The possibility exists that our observations and/or analysis techniques have introduced a systematic error in our derived initial or final masses. As described in Section 2.2.3, all three M67 non-DAs included in the IFMR have some oddity in either the spectral fits or the resulting parameters. We have double-checked the data and reductions from these stars and others observed on the same night with the same setup, and we do not see evidence for any obvious systematic error.

As discussed by Salaris et al. (2009) and illustrated clearly by Cummings et al. (2018), a precision IFMR should be constructed from self-consistent models and analysis. The non-DA IFMR we present is not produced in a fully consistent manner. Our WD parameters come from a mixture of photometric and spectroscopic fits, except for Procyon B, which has an astrometrically measured mass. Our adopted star cluster ages are generally derived from isochrone fitting using PARSEC isochrones, but the Procyon system age was derived from a combination of asteroseismological measurements with stellar evolutionary models, though for the sake of consistency we prefer the age derived using PARSEC models.

As mentioned previously, the spectral models for non-DA WDs contain complex physics that is not fully understood and are currently undergoing cycles of revision, and potentially this could bias our results. For example, we have not applied 3D corrections to WD spectroscopic parameters proposed by Cukanovaite et al. (2021), as their corrections are likely to change as additional and improved microphysical calculations are included in model atmospheres. Yet these same systematics should also affect the mass determinations of non-DA field WDs – and the mean masses and dispersions of field DA and DB WDs are not significantly different (e.g., Genest-Beaulieu & Bergeron 2019b).

Conservatively, our analysis may be biased by overconfidence in our use of Procyon B in the non-DA IFMR. If we ignore Procyon B, then the significance of any difference between the DA and non-DA semi-empirical IFMRs is greatly reduced and could be explained away as being due to small number statistics. As described above, there are reasons to be suspicious of the inclusion of Procyon B in an IFMR analysis, since we are not certain that its past interactions with Procyon A were negligible.

Additional non-DA WDs are clearly needed to be studied and added to the non-DA semi-empirical IFMR if we are to confirm or refute the potential differences between the IFMRs. Because of the relative rarity of non-DA WDs and because of the exquisite observations required for spectral fitting, progress is likely to be slow if we limit ourselves to analysis of high signal-to-noise spectral observations of open cluster non-DA WDs. Two alternative observational strategies may permit more efficient progress to be made on the non-DA IFMR. First, common proper motion binaries with a non-

DA WD component may be more numerous than open cluster non-DA WDs once Gaia results are thoroughly searched. The IFMR constructed from these binaries tends to have larger uncertainty in M_i due to more uncertain ages of the binary companion, but sample size can overcome this drawback.

Second, for non-DA WDs there has been substantial progress in obtaining precision WD T_{eff} and $\log g$ from multi-band photometric modeling, especially if near UV photometry is available outside of the Rayleigh-Jeans tail of the WD spectral energy distribution. Combined with astrometric confirmation that a given WD is a member of a cluster or a wide binary, these photometric models may reduce the need for very high signal-to-noise optical spectroscopy (Genest-Beaulieu & Bergeron 2019b,a). However, some spectroscopy is likely to remain necessary in order to confirm the non-DA nature of candidate WDs and to provide reasonable limits on the H abundance in the WD atmosphere.

4.3. Conclusions

In this paper, we have presented results from a study of the semi-empirical IFMR for non-DA WDs. As our discussions touched on several subjects, we summarize our main conclusions here.

- We present a sample of non-DA WDs that are known astrometric members of open star clusters or, in the case of Procyon B, a component in a well-studied binary system. For those WDs without previously published spectral parameters, we present spectroscopic and photometric fits to synthetic atmospheres in order to determine T_{eff} , $\log g$, and associated uncertainties in each parameter. Using DB evolutionary models to determine τ_{cool} for each WD in the sample, we construct a semi-empirical IFMR for non-DA WDs.
- Because the uncertainties in the initial-final mass plane are highly correlated, we conducted Monte Carlo simulations of both the true uncertainties in the parameters derived for individual WDs and in the shape and location of the ensemble semi-empirical IFMR. We find that the correlated errors for individual WDs are non-Gaussian and non-symmetric, but when a large sample of WDs is considered, the inferred semi-empirical IFMR is not greatly biased in spite of the correlated errors in M_f and M_i . This conclusion holds true for both DA and non-DA WDs.
- The non-DA IFMR is mildly inconsistent with published semi-empirical DA IFMRs; the non-DA WDs appear to be roughly $0.07 M_{\odot}$ less massive for a given initial mass than DA WDs. If physical, this offset could be due to unexpected enhanced mass loss from the WDs during the thermal pulse and renewed post-AGB evolution of the star. This offset is significantly larger than models and observations of mass loss during LTPs and VLTPs, and it is inconsistent with the observed agreement of the mean masses of DA and non-DA field WDs.

We are therefore skeptical that the apparent difference in the DA and non-DA IFMRs is physically real.

- The apparent differences in the IFMRs may be biased by the inclusion of Procyon B in the sample. Procyon B has been previously noted as being inconsistent with the semi-empirical IFMR. Potential past binary interactions between Procyon A & B may explain its discrepant point in the IFMR.
- A significantly larger sample size of non-DA WDs is needed to determine whether or not the non-DA IFMR differs from that of the DA IFMR. If there is indeed a significant difference, this would imply part of our understanding of the progenitors of non-DA WDs is incomplete.

The authors wish to recognize and acknowledge the very significant cultural role and reverence that the summit of Maunakea has always had within the indigenous Hawaiian community. We are most fortunate to have the opportunity to conduct observations from this mountain.

This work has been supported by the National Science Foundation under grants awards AST-1910551 and AST-0602288, and supported by Cottrell College Science Award 22706 from the Research Corporation for Science Advancement. A.B. acknowledges support from the Natural Sciences and Engineering Research Council (NSERC) of Canada through an Alexander Graham Bell Graduate Scholarship.

J. Barnett is grateful for the service of M. Wood and K. Montgomery on his M.S. thesis committee and for their helpful comments and suggestions during this project. The authors also thank Pierre Bergeron for his assistance in setting up this collaboration. The authors also thank the anonymous referee for her/his efforts and suggestions. The exquisite observing skills of K.H.R. Rubin were crucial to the success of this project.

Facility: Keck I (LRIS-B)

Software: IRAF (Tody 1986, 1993)

REFERENCES

- | | |
|---|---|
| <p>Ahumada, R., Prieto, C. A., Almeida, A., et al. 2020, ApJS, 249, 3,
doi: 10.3847/1538-4365/ab929e</p> <p>Althaus, L. G., Miller Bertolami, M. M., & Córscico, A. H. 2013, A&A, 557, A19,
doi: 10.1051/0004-6361/201321868</p> <p>Althaus, L. G., Panei, J. A., Miller Bertolami, M. M., et al. 2009, ApJ, 704, 1605,
doi: 10.1088/0004-637X/704/2/1605</p> | <p>Althaus, L. G., Serenelli, A. M., Panei, J. A., et al. 2005, A&A, 435, 631,
doi: 10.1051/0004-6361:20041965</p> <p>Arendt, R. G. 2006, density.pro, 1.4.
https://www.stsci.edu/~robberto/Main/Software/IDL4pipeline/index.html</p> <p>Bédard, A., Bergeron, P., Brassard, P., & Fontaine, G. 2020, ApJ, 901, 93,
doi: 10.3847/1538-4357/abafbe</p> |
|---|---|

- Bellini, A., Bedin, L. R., Piotto, G., et al. 2010, *A&A*, 513, A50, doi: [10.1051/0004-6361/200913721](https://doi.org/10.1051/0004-6361/200913721)
- Bergeron, P., Dufour, P., Fontaine, G., et al. 2019, *ApJ*, 876, 67, doi: [10.3847/1538-4357/ab153a](https://doi.org/10.3847/1538-4357/ab153a)
- Bergeron, P., Saffer, R. A., & Liebert, J. 1992, *ApJ*, 394, 228, doi: [10.1086/171575](https://doi.org/10.1086/171575)
- Bergeron, P., Wesemael, F., Dufour, P., et al. 2011, *ApJ*, 737, 28, doi: [10.1088/0004-637X/737/1/28](https://doi.org/10.1088/0004-637X/737/1/28)
- Blouin, S., Dufour, P., Thibeault, C., & Allard, N. F. 2019, *ApJ*, 878, 63, doi: [10.3847/1538-4357/ab1f82](https://doi.org/10.3847/1538-4357/ab1f82)
- Bonatto, C., Campos, F., Kepler, S. O., & Bica, E. 2015, *MNRAS*, 450, 2500, doi: [10.1093/mnras/stv822](https://doi.org/10.1093/mnras/stv822)
- Bond, H. E., Gilliland, R. L., Schaefer, G. H., et al. 2018, *Research Notes of the American Astronomical Society*, 2, 147, doi: [10.3847/2515-5172/aad9a4](https://doi.org/10.3847/2515-5172/aad9a4)
- . 2015, *ApJ*, 813, 106, doi: [10.1088/0004-637X/813/2/106](https://doi.org/10.1088/0004-637X/813/2/106)
- Bressan, A., Marigo, P., Girardi, L., et al. 2012, *MNRAS*, 427, 127, doi: [10.1111/j.1365-2966.2012.21948.x](https://doi.org/10.1111/j.1365-2966.2012.21948.x)
- Chambers, K. C., Magnier, E. A., Metcalfe, N., et al. 2016, arXiv e-prints, arXiv:1612.05560, <https://arxiv.org/abs/1612.05560>
- Chen, Y., Bressan, A., Girardi, L., et al. 2015, *MNRAS*, 452, 1068, doi: [10.1093/mnras/stv1281](https://doi.org/10.1093/mnras/stv1281)
- Chen, Y., Girardi, L., Bressan, A., et al. 2014, *MNRAS*, 444, 2525, doi: [10.1093/mnras/stu1605](https://doi.org/10.1093/mnras/stu1605)
- Clayton, G. C., & De Marco, O. 1997, *AJ*, 114, 2679, doi: [10.1086/118678](https://doi.org/10.1086/118678)
- Clayton, G. C., Kerber, F., Pirzkal, N., et al. 2006, *ApJL*, 646, L69, doi: [10.1086/506593](https://doi.org/10.1086/506593)
- Clayton, G. C., Bond, H. E., Long, L. A., et al. 2013, *ApJ*, 771, 130, doi: [10.1088/0004-637X/771/2/130](https://doi.org/10.1088/0004-637X/771/2/130)
- Coutu, S., Dufour, P., Bergeron, P., et al. 2019, *ApJ*, 885, 74, doi: [10.3847/1538-4357/ab46b9](https://doi.org/10.3847/1538-4357/ab46b9)
- Cukanovaite, E., Tremblay, P.-E., Bergeron, P., et al. 2021, *MNRAS*, 501, 5274, doi: [10.1093/mnras/staa3684](https://doi.org/10.1093/mnras/staa3684)
- Cukanovaite, E., Tremblay, P. E., Freytag, B., Ludwig, H. G., & Bergeron, P. 2018, *MNRAS*, 481, 1522, doi: [10.1093/mnras/sty2383](https://doi.org/10.1093/mnras/sty2383)
- Cummings, J. D., Kalirai, J. S., Choi, J., et al. 2019, *ApJL*, 871, L18, doi: [10.3847/2041-8213/aafc2d](https://doi.org/10.3847/2041-8213/aafc2d)
- Cummings, J. D., Kalirai, J. S., Tremblay, P.-E., & Ramirez-Ruiz, E. 2015, *ApJ*, 807, 90, doi: [10.1088/0004-637X/807/1/90](https://doi.org/10.1088/0004-637X/807/1/90)
- Cummings, J. D., Kalirai, J. S., Tremblay, P. E., Ramirez-Ruiz, E., & Choi, J. 2018, *ApJ*, 866, 21, doi: [10.3847/1538-4357/aadfd6](https://doi.org/10.3847/1538-4357/aadfd6)
- Cunningham, T., Tremblay, P.-E., Gentile Fusillo, N. P., Hollands, M., & Cukanovaite, E. 2020, *MNRAS*, 492, 3540, doi: [10.1093/mnras/stz3638](https://doi.org/10.1093/mnras/stz3638)
- Demarque, P., Guenther, D. B., Li, L. H., Mazumdar, A., & Straka, C. W. 2008, *Ap&SS*, 316, 31, doi: [10.1007/s10509-007-9698-y](https://doi.org/10.1007/s10509-007-9698-y)
- Duerbeck, H. W., & Benetti, S. 1996, *ApJL*, 468, L111, doi: [10.1086/310241](https://doi.org/10.1086/310241)
- Eggen, O. J. 1984, *AJ*, 89, 830, doi: [10.1086/113578](https://doi.org/10.1086/113578)
- Evans, A., Gehrz, R. D., Woodward, C. E., et al. 2020, *MNRAS*, 493, 1277, doi: [10.1093/mnras/staa343](https://doi.org/10.1093/mnras/staa343)
- Fabricius, C., Luri, X., Arenou, F., et al. 2020, arXiv e-prints, arXiv:2012.06242, <https://arxiv.org/abs/2012.06242>
- Falcon, R. E., Winget, D. E., Montgomery, M. H., & Williams, K. A. 2010, *ApJ*, 712, 585, doi: [10.1088/0004-637X/712/1/585](https://doi.org/10.1088/0004-637X/712/1/585)
- . 2012, *ApJ*, 757, 116, doi: [10.1088/0004-637X/757/2/116](https://doi.org/10.1088/0004-637X/757/2/116)
- Ferrario, L., Wickramasinghe, D., Liebert, J., & Williams, K. A. 2005, *MNRAS*, 361, 1131, doi: [10.1111/j.1365-2966.2005.09244.x](https://doi.org/10.1111/j.1365-2966.2005.09244.x)

- Fleming, T. A., Liebert, J., Bergeron, P., & Beauchamp, A. 1997, in *Astrophysics and Space Science Library*, Vol. 214, White dwarfs, ed. J. Isern, M. Hernanz, & E. Garcia-Berro, 91, doi: [10.1007/978-94-011-5542-7_15](https://doi.org/10.1007/978-94-011-5542-7_15)
- Gaia Collaboration, Brown, A. G. A., Vallenari, A., et al. 2020, arXiv e-prints, arXiv:2012.01533. <https://arxiv.org/abs/2012.01533>
- Gaia Collaboration, Babusiaux, C., van Leeuwen, F., et al. 2018a, *A&A*, 616, A10, doi: [10.1051/0004-6361/201832843](https://doi.org/10.1051/0004-6361/201832843)
- Gaia Collaboration, Brown, A. G. A., Vallenari, A., et al. 2018b, *A&A*, 616, A1, doi: [10.1051/0004-6361/201833051](https://doi.org/10.1051/0004-6361/201833051)
- García-Berro, E., Althaus, L. G., Córscico, A. H., & Isern, J. 2008, *ApJ*, 677, 473, doi: [10.1086/527536](https://doi.org/10.1086/527536)
- Genest-Beaulieu, C., & Bergeron, P. 2019a, *ApJ*, 882, 106, doi: [10.3847/1538-4357/ab379e](https://doi.org/10.3847/1538-4357/ab379e)
- . 2019b, *ApJ*, 871, 169, doi: [10.3847/1538-4357/aafac6](https://doi.org/10.3847/1538-4357/aafac6)
- Gomez, T. A., Nagayama, T., Fontes, C. J., et al. 2020, *PhRvL*, 124, 055003, doi: [10.1103/PhysRevLett.124.055003](https://doi.org/10.1103/PhysRevLett.124.055003)
- Gonzalez, G., Lambert, D. L., Wallerstein, G., et al. 1998, *ApJS*, 114, 133, doi: [10.1086/313068](https://doi.org/10.1086/313068)
- Greenstein, J. L. 1976, *ApJ*, 210, 524, doi: [10.1086/154856](https://doi.org/10.1086/154856)
- Guenther, D. B., Demarque, P., & Gruberbauer, M. 2014, *ApJ*, 787, 164, doi: [10.1088/0004-637X/787/2/164](https://doi.org/10.1088/0004-637X/787/2/164)
- Guerrero, M. A., Fang, X., Miller Bertolami, M. M., et al. 2018, *Nature Astronomy*, 2, 784, doi: [10.1038/s41550-018-0551-8](https://doi.org/10.1038/s41550-018-0551-8)
- Harris, H. C., Munn, J. A., Kilic, M., et al. 2006, *AJ*, 131, 571, doi: [10.1086/497966](https://doi.org/10.1086/497966)
- Iben, Jr., I., Kaler, J. B., Truran, J. W., & Renzini, A. 1983, *ApJ*, 264, 605, doi: [10.1086/160631](https://doi.org/10.1086/160631)
- Iben, I., J., & Renzini, A. 1982, *ApJL*, 263, L23, doi: [10.1086/183916](https://doi.org/10.1086/183916)
- Kepler, S. O., Pelisoli, I., Koester, D., et al. 2019, *MNRAS*, 486, 2169, doi: [10.1093/mnras/stz960](https://doi.org/10.1093/mnras/stz960)
- Kervella, P., Thévenin, F., Morel, P., et al. 2004, *A&A*, 413, 251, doi: [10.1051/0004-6361:20031527](https://doi.org/10.1051/0004-6361:20031527)
- Kleinman, S. J., Kepler, S. O., Koester, D., et al. 2013, *ApJS*, 204, 5, doi: [10.1088/0067-0049/204/1/5](https://doi.org/10.1088/0067-0049/204/1/5)
- Koester, D., & Kepler, S. O. 2015, *A&A*, 583, A86, doi: [10.1051/0004-6361/201527169](https://doi.org/10.1051/0004-6361/201527169)
- Koester, D., Voss, B., Napiwotzki, R., et al. 2009, *A&A*, 505, 441, doi: [10.1051/0004-6361/200912531](https://doi.org/10.1051/0004-6361/200912531)
- Lau, H. H. B., De Marco, O., & Liu, X. W. 2011, *MNRAS*, 410, 1870, doi: [10.1111/j.1365-2966.2010.17568.x](https://doi.org/10.1111/j.1365-2966.2010.17568.x)
- Lawlor, T. M., & MacDonald, J. 2003, *ApJ*, 583, 913, doi: [10.1086/345411](https://doi.org/10.1086/345411)
- Liebert, J., Bergeron, P., & Holberg, J. B. 2005, *ApJS*, 156, 47, doi: [10.1086/425738](https://doi.org/10.1086/425738)
- Liebert, J., Fontaine, G., Young, P. A., Williams, K. A., & Arnett, D. 2013, *ApJ*, 769, 7, doi: [10.1088/0004-637X/769/1/7](https://doi.org/10.1088/0004-637X/769/1/7)
- Lindgren, L., Klioner, S. A., Hernández, J., et al. 2020, arXiv e-prints, arXiv:2012.03380. <https://arxiv.org/abs/2012.03380>
- Marigo, P., Bressan, A., Nanni, A., Girardi, L., & Pumo, M. L. 2013, *MNRAS*, 434, 488, doi: [10.1093/mnras/stt1034](https://doi.org/10.1093/mnras/stt1034)
- Marigo, P., Girardi, L., Bressan, A., et al. 2008, *A&A*, 482, 883, doi: [10.1051/0004-6361:20078467](https://doi.org/10.1051/0004-6361:20078467)
- McCarthy, J. K., Cohen, J. G., Butcher, B., et al. 1998, in *Proc. SPIE*, Vol. 3355, *Optical Astronomical Instrumentation*, ed. S. D'Odorico, 81–92, doi: [10.1117/12.316831](https://doi.org/10.1117/12.316831)
- McCook, G. P., & Sion, E. M. 1999, *ApJS*, 121, 1, doi: [10.1086/313186](https://doi.org/10.1086/313186)
- Montgomery, M. H., Winget, D. E., Schaeuble, M. A., Dunlap, B. H., & Fuchs, J. T. 2020, in *Laboratory Astrophysics: From Observations to Interpretation*, ed. F. Salama & H. Linnartz, Vol. 350, 231–236, doi: [10.1017/S1743921320000599](https://doi.org/10.1017/S1743921320000599)

- Oke, J. B., Cohen, J. G., Carr, M., et al. 1995, *PASP*, 107, 375, doi: [10.1086/133562](https://doi.org/10.1086/133562)
- Parthasarathy, M., Garcia-Lario, P., Pottasch, S. R., et al. 1993, *A&A*, 267, L19
- Provencal, J. L., Shipman, H. L., Koester, D., Wesemael, F., & Bergeron, P. 2002, *ApJ*, 568, 324, doi: [10.1086/338769](https://doi.org/10.1086/338769)
- Reindl, N., Rauch, T., Miller Bertolami, M. M., Todt, H., & Werner, K. 2017, *MNRAS*, 464, L51, doi: [10.1093/mnrasl/slw175](https://doi.org/10.1093/mnrasl/slw175)
- Reindl, N., Rauch, T., Parthasarathy, M., et al. 2014, *A&A*, 565, A40, doi: [10.1051/0004-6361/201323189](https://doi.org/10.1051/0004-6361/201323189)
- Richer, H. B., Kerr, R., Heyl, J., et al. 2019, *ApJ*, 880, 75, doi: [10.3847/1538-4357/ab2874](https://doi.org/10.3847/1538-4357/ab2874)
- Rockosi, C., Stover, R., Kibrick, R., et al. 2010, in *Proc. SPIE*, Vol. 7735, Ground-based and Airborne Instrumentation for Astronomy III, 77350R, doi: [10.1117/12.856818](https://doi.org/10.1117/12.856818)
- Rolland, B., Bergeron, P., & Fontaine, G. 2018, *ApJ*, 857, 56, doi: [10.3847/1538-4357/aab713](https://doi.org/10.3847/1538-4357/aab713)
- Rubin, K. H. R., Williams, K. A., Bolte, M., & Koester, D. 2008, *AJ*, 135, 2163, doi: [10.1088/0004-6256/135/6/2163](https://doi.org/10.1088/0004-6256/135/6/2163)
- Sahlholdt, C. L., Feltzing, S., Lindegren, L., & Church, R. P. 2019, *MNRAS*, 482, 895, doi: [10.1093/mnras/sty2732](https://doi.org/10.1093/mnras/sty2732)
- Salaris, M., Serenelli, A., Weiss, A., & Bertolami, M. M. 2009, *The Astrophysical Journal*, 692, 1013, doi: [10.1088/0004-637x/692/2/1013](https://doi.org/10.1088/0004-637x/692/2/1013)
- Schaefer, B. E., Bond, H. E., & Sahu, K. C. 2020, arXiv e-prints, arXiv:2012.04223, <https://arxiv.org/abs/2012.04223>
- Schaeuble, M. A., Nagayama, T., Bailey, J. E., et al. 2019, *ApJ*, 885, 86, doi: [10.3847/1538-4357/ab479d](https://doi.org/10.3847/1538-4357/ab479d)
- Schoenberner, D. 1979, *A&A*, 79, 108
- Tody, D. 1986, in *Proc. SPIE*, Vol. 627, Instrumentation in astronomy VI, ed. D. L. Crawford, 733, doi: [10.1117/12.968154](https://doi.org/10.1117/12.968154)
- Tody, D. 1993, in *Astronomical Society of the Pacific Conference Series*, Vol. 52, *Astronomical Data Analysis Software and Systems II*, ed. R. J. Hanisch, R. J. V. Brissenden, & J. Barnes, 173
- Tremblay, P., Beauchamp, A., & Bergeron, P. 2020, *ApJ*, 901, 104, doi: [10.3847/1538-4357/abb0e5](https://doi.org/10.3847/1538-4357/abb0e5)
- Tremblay, P. E., Cukanovaite, E., Gentile Fusillo, N. P., Cunningham, T., & Hollands, M. A. 2019, *MNRAS*, 482, 5222, doi: [10.1093/mnras/sty3067](https://doi.org/10.1093/mnras/sty3067)
- Tremblay, P.-E., Schilbach, E., Röser, S., et al. 2012, *A&A*, 547, A99, doi: [10.1051/0004-6361/201220057](https://doi.org/10.1051/0004-6361/201220057)
- Werner, K., & Herwig, F. 2006, *PASP*, 118, 183, doi: [10.1086/500443](https://doi.org/10.1086/500443)
- Williams, K. A. 2020, *IAU Symposium*, 357, 179, doi: [10.1017/S1743921320000848](https://doi.org/10.1017/S1743921320000848)
- Williams, K. A., & Bolte, M. 2007, *AJ*, 133, 1490, doi: [10.1086/511675](https://doi.org/10.1086/511675)
- Williams, K. A., Bolte, M., & Koester, D. 2009, *ApJ*, 693, 355, doi: [10.1088/0004-637X/693/1/355](https://doi.org/10.1088/0004-637X/693/1/355)
- Williams, K. A., Canton, P. A., Bellini, A., et al. 2018, *ApJ*, 867, 62, doi: [10.3847/1538-4357/aad90b](https://doi.org/10.3847/1538-4357/aad90b)
- Williams, K. A., Liebert, J., Bolte, M., & Hanson, R. B. 2006, *ApJL*, 643, L127, doi: [10.1086/505211](https://doi.org/10.1086/505211)